Electronic Supplementary Information for:

Examining the effect of manganese distribution on alcohol production in $CoMn/TiO_2$ FTS catalysts

Jay M. Pritchard[1,2], Matthew Lindley[3] , Danial Farooq[1,2], Urvashi Vyas[1,2], Sarah J. Haigh[3], James Paterson[4], Mark Peacock[4], Andrew M. Beale[1,2]

[1]*Department of Chemistry, University College London, 20 Gordon Street, WC1H 0AJ, UK*

[2]*Research Complex at Harwell, Rutherford Appleton Laboratories, Harwell Science and Innovation Campus, Harwell, Didcot, OX11 0FA, UK*

[3]*Department of Materials, University of Manchester, Manchester M13 9PL, UK*

[4]*BP, Applied Sciences, Innovation & Engineering, Saltend, Hull, UK*

1. XRD data

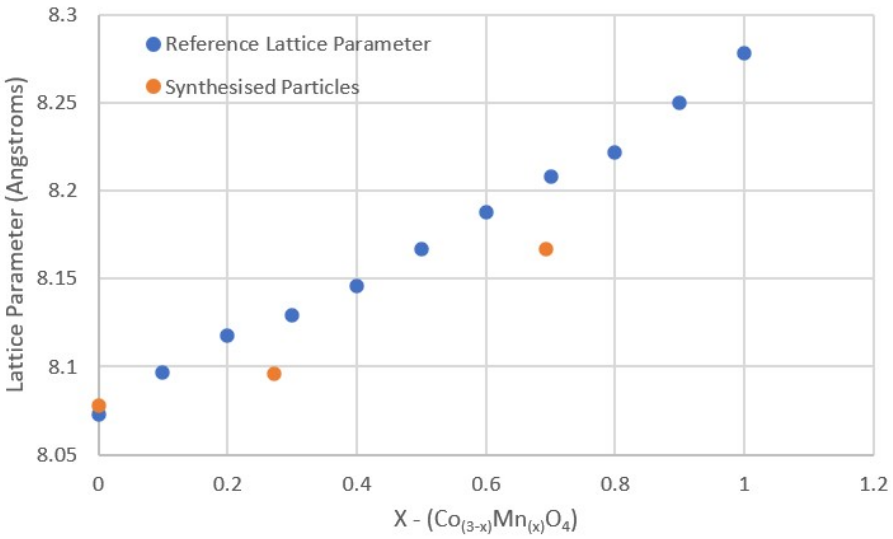

Figure S1. Lattice Parameter of $Co_{(3-x)}Mn_{(x)}O_4$ for varying x from reference literature adapted from Meena et al., and synthesised mixed oxide nanoparticle series with varying Mn doping.[1]

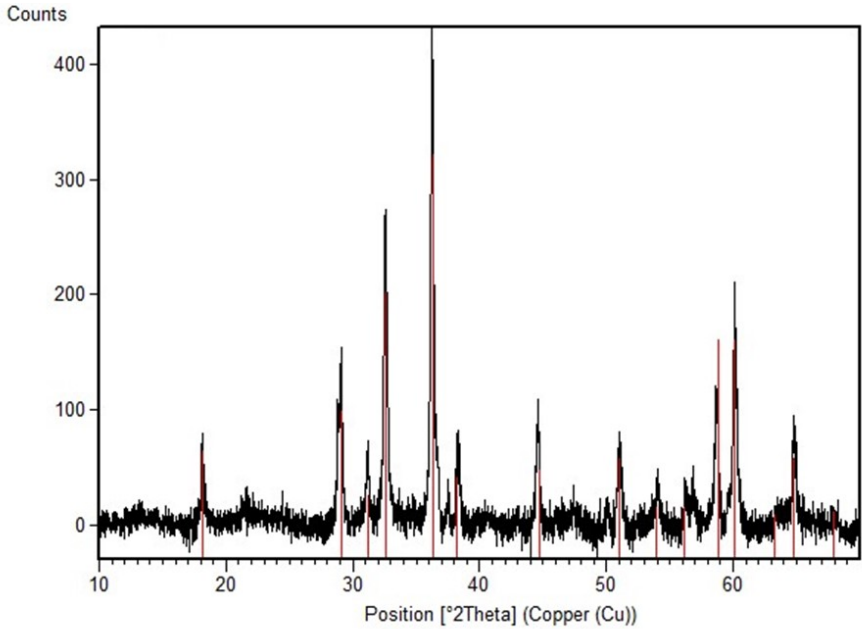

Figure S2. Background subtracted diffraction pattern of synthesised sample Mn_3O_4, with the reflections of the tetragonal spinel phase (Hausmannite) indicated in red.[2]

Figure S2 shows the diffractogram of the hydrothermal synthesis with manganese in the absence of cobalt. The resulting brown solid was filtered and purified, and the measured diffraction pattern corresponds to tetragonal Mn_3O_4, Hausmannite.[2] The sample produced was used to synthesise catalysts with physical mixtures of Co_3O_4 / Mn_3O_4 supported particles.

Table S1 — Rietveld refined parameters for surface coated particles supported on TiO_2.

Co:Mn	Lattice Parameter (Å)	% expansion
0	8.078	-
100:1	8.081	0.04
100:5	8.077	-0.01
100:10	8.086	0.10
100:30	8.084	0.07

2. XPS

To further investigate the potential of interaction between the doped manganese and cobalt in the synthesised particles, a small number of samples were studied by XPS. As the binding energies measured by XPS are affected by the local chemical environment of the atoms, any variation identified between doping methods or loadings may be indicative of the effectiveness of the synthesis goals. The Co 2p transitions for the measured samples are shown in Figure . The synthesised Co_3O_4 species shows reasonable consistency in peak position with the synthesised 100:10 Co:Mn (10 wt% Co_3O_4/1 wt% Mn_3O_4) mixed oxide species, while there is a minor shift in binding energy for the sample with higher manganese content of 100:30 Co:Mn (10 wt% Co_3O_4/3 wt% Mn_3O_4).

For the Co_3O_4 and 100:10 Co:Mn mixed oxide samples, the peak positions of 780.0 & 795.25 eV in Figure S3 correspond well to the reported binding energies for $2p_{3/2}$ and $2p_{1/2}$ respectively for Co_3O_4.[11]

Meanwhile, a shift to higher binding energy for the 100:30 mixed oxide sample, to 780.5 & 796.25 eV is observed.

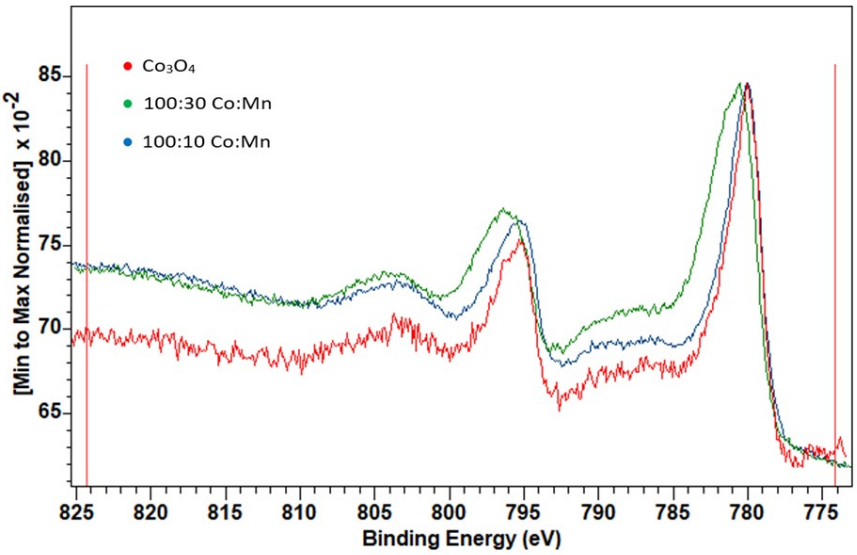

Figure S3. XPS spectra of Co_3O_4, the 100:30 mixed oxide & 100:10 mixed oxide samples covering the Co 2p region.

Figure S4 shows the XPS spectra for Mn_3O_4, the 100:30 & 100:10 mixed oxide samples for the Mn 2p transitions. For the synthesised Mn_3O_4, the peak positions of 641.5 eV & 653.25 eV correspond to the reported binding energies for $2p_{3/2}$ and $2p_{1/2}$ respectively for Mn_3O_4.[22] While a minor shift in peak position is observed for the mixed oxide samples, the biggest change in the profile is for the 100:10 mixed oxide sample where a broadening of the binding energy towards higher energies is observed. This shift suggests an increase in the ratio of Mn^{3+} present within the sample, suggesting the potential preferential occupation of the manganese within the octahedral sites of the spinel structure at this lower % Mn loading. [12]

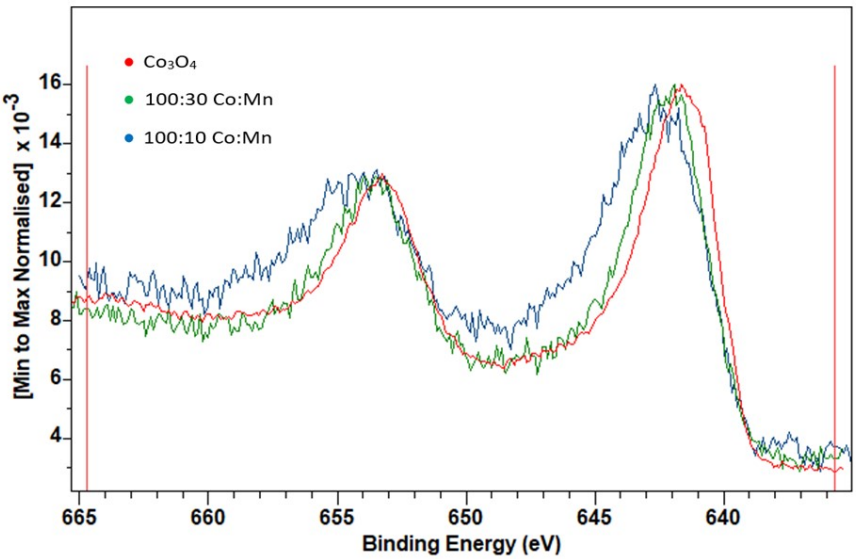

Figure S4. XPS spectra of Co_3O_4, the 100:30 mixed oxide & 100:10 mixed oxide samples covering the Mn 2p region.

Table S2 shows the relative quantification of Co and Mn by fitting of high resolution XPS measurements taken in the 2p regions for each element. The two samples studied, (Co:Mn) 100:30 surface doped & 100:30 mixed oxide have nominally the same ratio of Co:Mn, 100:30. As XPS is a surface sensitive technique rather than a bulk measurement, we would expect to see the calculated loadings to be dependent on the order of the metals within the synthesised nanoparticles. The quantification of 83.7 % Mn at the surface of the surface doped sample suggests the manganese is effectively distributed over the surface of the cobalt, and obscuring the majority of the cobalt content from quantification with only 16.3 % being measured. Meanwhile, the mixed oxide 100:30 sample shows good consistency with the nominal loadings, with the measured 24.3 % Mn closely corresponding to the nominal loading of 23.1 %.

Table S2 – Relative Quantification of Co and Mn phases by fitting of XPS results.

Doping Method	**Co:Mn**	**% Co**	**% Mn**
Surface doped	100:30	16.3	83.7
Mixed oxide	100:30	75.7	24.3

3. STEM

Figure S6 shows the Ti K Series and Co K series SEM EDX maps of Co_3O_4 particles dispersed over TiO_2. The aim of this mapping is to understand how effectively the supporting method is in distributing the synthesised cobalt oxide particles on the titania support. The distribution of Ti and Co within the maps show similar distribution for each element, suggest that the experimental method for the supporting of the particles is effective in achieving a well-mixed system.

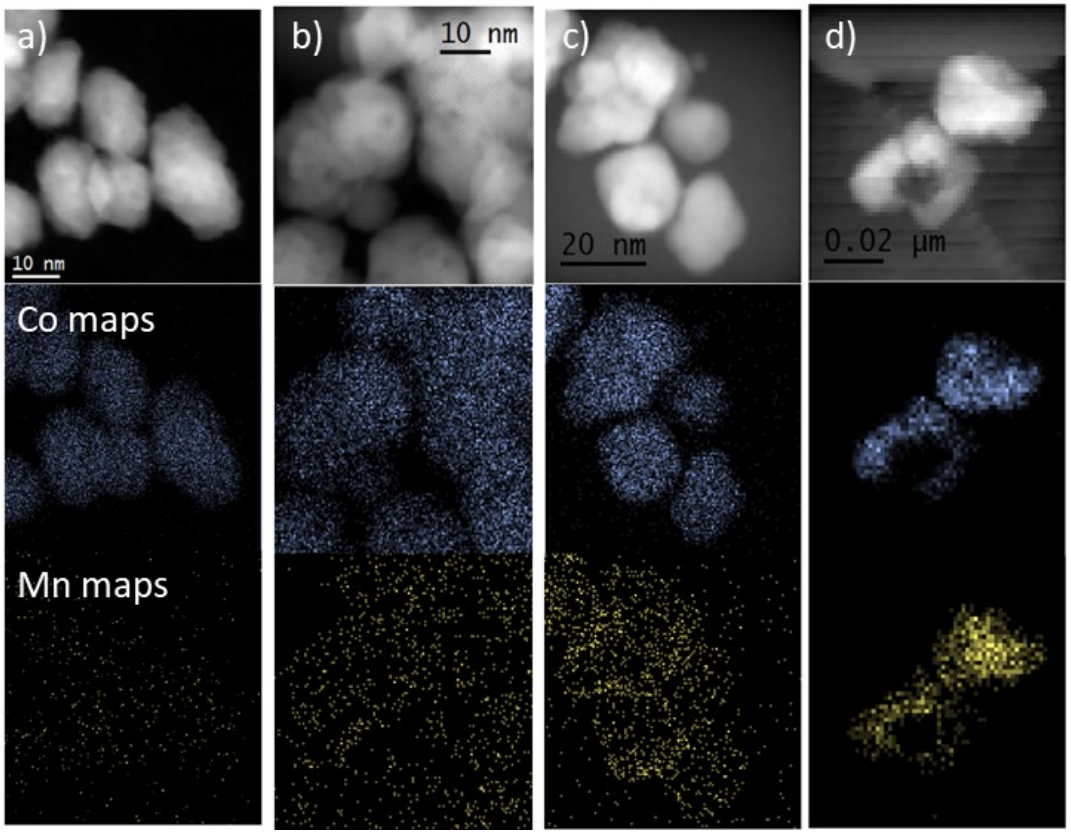

Figure S5. STEMHAADF images (top row), Co (middle row) and Mn (bottom row) STEM-EDX elemental maps of sample a) surface doped (Co:Mn) 100:1, b) surface doped (Co:Mn) 100:5, c) surface doped (Co:Mn) 100:10 and d) mixed oxide $Co_2Mn_1O_4$. All samples show a tendency for Mn enrichment to occur at the particle surface but the effect is much greater in the surface doped materials.

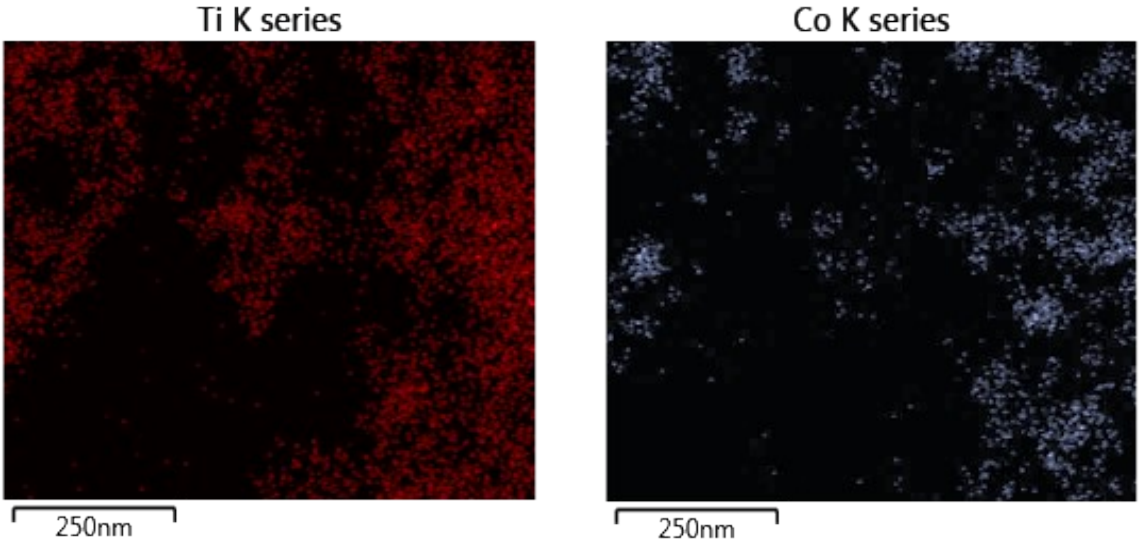

Figure S6. Ti and Co K-edge, low magnification STEM maps of Co_3O_4 dispersed on TiO_2. Note the results suggest an even dispersion of the two elements, indicative of a good dispersion of the Co_3O_4 over the TiO_2 surface.

4. HAADF/EELS

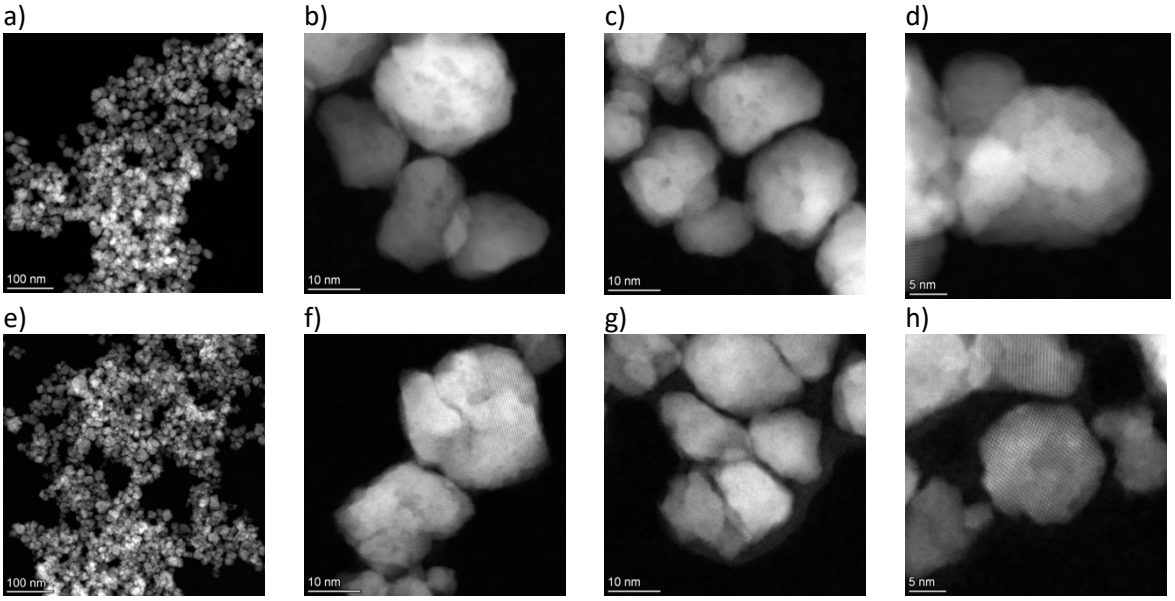

Figure S7. STEM HAADF imaging performed on fresh catalysts: a) – d) Co:Mn 100:30 surface doped and e) – h) mixed oxide $Co_{2.3}Mn_{0.7}O_4$ with ca. 20 nm crystal size.

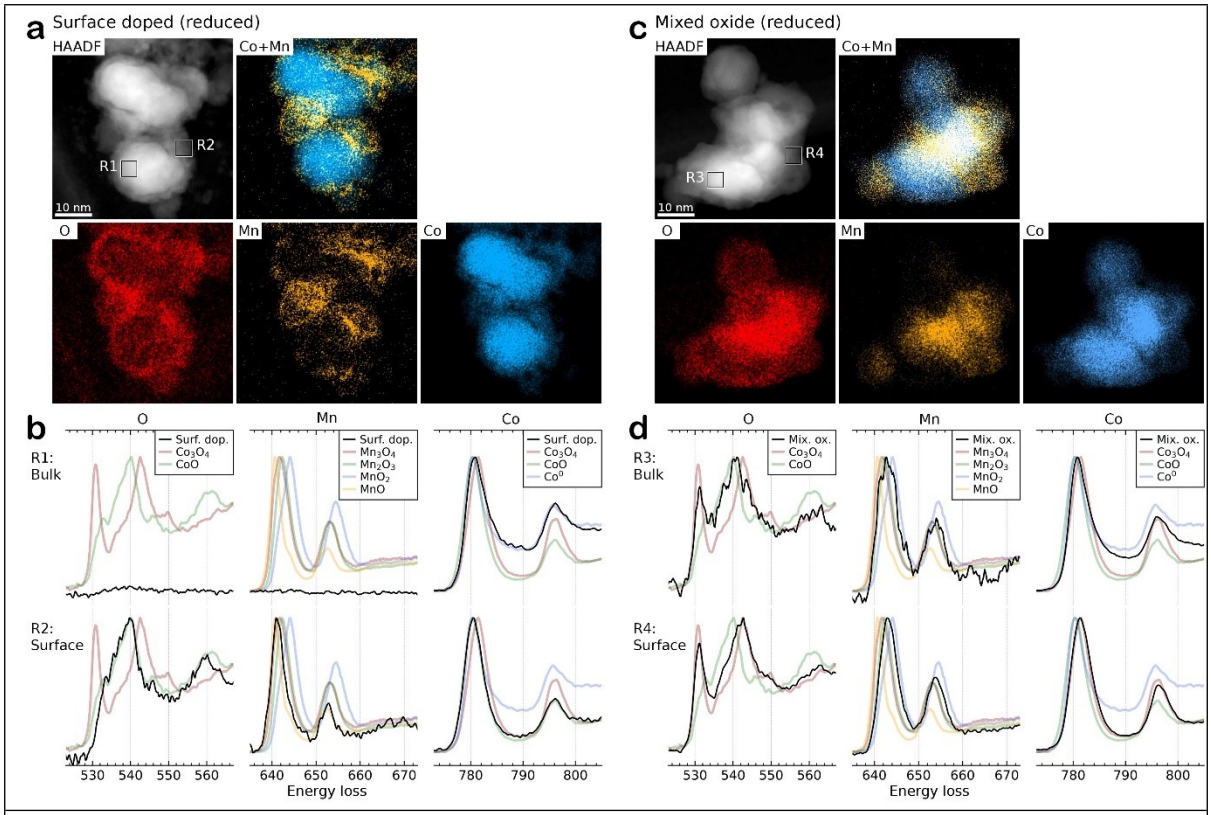

Figure S8. Representative HAADF imaging, EDS elemental mapping, and EELS oxidation state probing from the unsupported, reduced (a,b) surface doped 100:30 and (b,c) mixed oxide $Co_{2.3}Mn_{0.7}O_4$ samples. For the STEM-EELS in (b,c) reference spectra from various Co and Mn reference oxides and metallic species were collected for comparison. PCA deconvolution of the Co and Mn spectra was performed to identify the predominant species present. Note deconvolution of the O K-edge spectra was not performed due to overlapping contributions from Co and Mn species.

5. Performance testing

Figure S9 shows the relationship between alcohol selectivity and the outlet H_2:CO. Given that the inlet H_2:CO is nominally 1.81, the outlet H_2:CO is expected to be lower than this across the tested catalysts. The value at the reactor outlet is dependent on the consumption ratio of the tested catalyst and the conversion rate, however the H_2:CO is also influenced by WGS activity. In the catalysts with high alcohol selectivity, we can see the outlet H_2:CO is consistently high, above 1.7. The model catalyst samples studied are supported on P25, a non-porous support. As such the localised H_2:CO experienced by the active catalyst is not expected to vary due to gas diffusion or mass transfer limitations of the synthesised products.

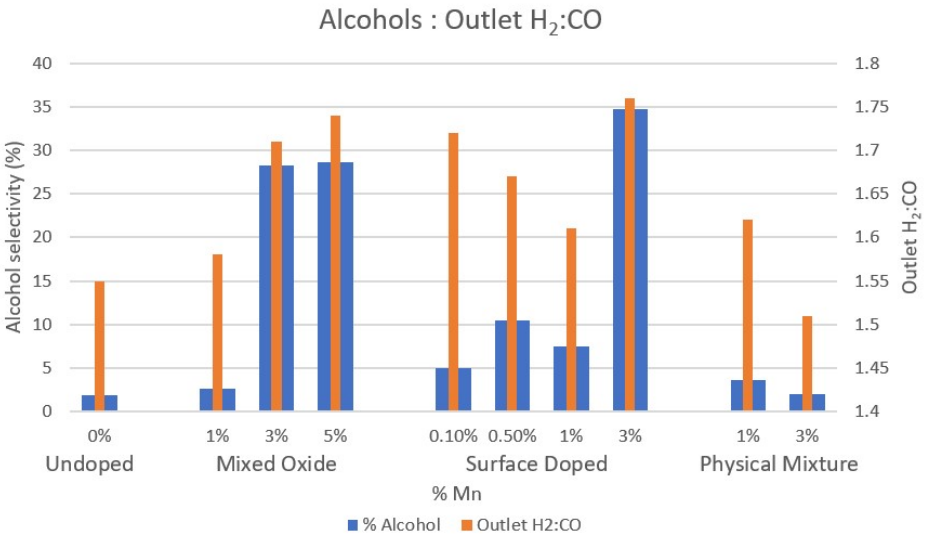

Figure S9. Alcohol selectivity, CO_2 selectivity (primary axis) and H_2:CO consumption (secondary axis) for each catalyst series tested.

References

1. Meena, P., Dielectric properties of spinel Co3-xMnxO4 (x= 0.1, 0.4, 0.7, and 1.0) ceramic compositions. *Indian Journal of Pure Applied Physics* **2015,** *52* (9), 625-631.
2. Aminoff, G., Ueber die Kristallstruktur von Hausmannit ($MnMn_2O_4$), *Zeitschrift fur Kristallographie* **1926**, *64*, 475-490.